Check for updates

Geophysical Research Letters

RESEARCH LETTER
10.1029/2023GL106599

Turbulence as a Key Driver of Ice Aggregation and Riming in Arctic Low-Level Mixed-Phase Clouds, Revealed by Long-Term Cloud Radar Observations

Giovanni Chellini[1] and **Stefan Kneifel**[2]

[1]Institute for Geophysics and Meteorology, University of Cologne, Cologne, Germany, [2]Meteorological Institute, Ludwig-Maximilians-Universität in Munich, Munich, Germany

Key Points:

- Relation between turbulence and ice growth investigated based on long-term remote sensing data set of Arctic low-level mixed-phase clouds
- Higher eddy dissipation rate (EDR) correlates with larger ice aggregates, and possibly higher degrees of fragmentation
- High EDR is an essential component needed for the formation of rimed particles

Supporting Information:

Supporting Information may be found in the online version of this article.

Correspondence to:

G. Chellini,
g.chellini@uni-koeln.de

Citation:

Chellini, G., & Kneifel, S. (2024). Turbulence as a key driver of ice aggregation and riming in Arctic low-level mixed-phase clouds, revealed by long-term cloud radar observations. *Geophysical Research Letters*, *51*, e2023GL106599. https://doi.org/10.1029/2023GL106599

Received 28 SEP 2023
Accepted 10 MAR 2024

Abstract Turbulence in clouds is known to enhance particle collision rates, as widely demonstrated for warm rain formation. A similar impact on ice growth processes is expected but a solid observational basis is missing. A statistical analysis of a 15-month data set of cloud radar observations allows for the first time to quantify the impact of turbulence on ice aggregation and riming in Arctic low-level mixed-phase clouds. Increasing eddy dissipation rate (EDR), from below 10^{-4} to above 10^{-3} m^2 s^{-3}, yields larger ice aggregates, and higher particle concentration, likely caused by increasing fragmentation. In conditions more favorable to riming, higher EDR is associated with dramatically higher particle fall velocities (by up to 125%), under similar liquid water paths, indicative of markedly higher degrees of riming. Our findings thus reveal the key role of turbulence for cold precipitation formation, and highlight the need for an improved understanding of turbulence-hydrometeor interactions in cold clouds.

Plain Language Summary Liquid and frozen precipitation mainly forms by collision and subsequent aggregation of small particles. Collisions between cloud particles, such as droplets and ice crystals, are thought to be increased by turbulence. While this effect has been intensively studied for liquid-only clouds, the impact of turbulence on ice-ice collisional growth (aggregation) and ice-liquid collisional growth (riming) is expected but has so far been poorly quantified. We study the effect of turbulence on aggregation and riming based on a long-term remote-sensing data set of low-level clouds containing both ice and liquid particles, recorded at the Arctic site of Ny-Ålesund, Svalbard. Cloud radar observations are used to retrieve the dissipation rate of turbulent kinetic energy (i.e., the eddy dissipation rate; EDR), which is the relevant quantity driving increases in collision rates, and to characterize ice particle properties. We find evidence that higher EDR regimes enhance the aggregation of particles, and are associated with signatures of increased ice particle concentration, possibly caused by the production of particle fragments upon collision. In temperature regimes more favorable to riming, turbulence dramatically enhances the particles' fall velocity, denoting higher degrees of riming. Our findings thus highlight a key role of turbulence for the formation of precipitable ice.

1. Introduction

Precipitation formation is for the most part determined by hydrometeor collisional processes: in warm clouds, hydrometeors transition from cloud droplets into drizzle and raindrops via the collision-coalescence process, while in cold clouds precipitation mainly forms by aggregation, that is, ice-ice collisions, and riming, that is, collisions between ice particles and supercooled droplets (Pruppacher & Klett, 2012). The role of turbulence in the initiation of warm precipitation has been widely debated in the past century (e.g., Arenberg, 1939; East & Marshall, 1954), and a consensus has been reached in recent decades on the key role it plays (e.g., Pumir & Wilkinson, 2016; Seifert & Onishi, 2016; Shaw, 2003). Conversely, the role of turbulence in collisional ice-growth processes has received little attention. A limited number of authors have suggested, based on case studies, that turbulence might induce enhancements in ice collisional growth (e.g., Aikins et al., 2016; Houze & Medina, 2005), and that increases in ice-ice collision rates might further affect precipitation by substantially enhancing secondary ice processes, especially collisional fragmentation (Billault-Roux et al., 2023; Ramelli et al., 2021). Consequently, turbulence represents a poorly understood pathway for the interaction between cloud dynamics and microphysics. Since most precipitation world-wide originates from the ice phase (Heymsfield et al., 2020; Mülmenstädt et al., 2015), a deeper understanding and quantitative estimate of the impact of turbulence on ice microphysical processes is likely to improve precipitation forecasts.

© 2024. The Authors.
This is an open access article under the terms of the Creative Commons Attribution License, which permits use, distribution and reproduction in any medium, provided the original work is properly cited.

19448007, 2024, 6, Downloaded from https://agupubs.onlinelibrary.wiley.com/doi/10.1029/2023GL106599 by Bibl. der Universitat zu Koln, Wiley Online Library on [12/11/2026]. See the Terms and Conditions (https://onlinelibrary.wiley.com/terms-and-conditions) on Wiley Online Library for rules of use; OA articles are governed by the applicable Creative Commons License

Theoretical fluid dynamics studies have shown dramatic increases in collision rates between particles suspended in a fluid with increasing turbulence. This effect is attributed to increasing modifications of particles trajectories by eddies on the smallest scales of the flow as the eddy dissipation rate (EDR) increases (e.g., Pumir & Wilkinson, 2016). When particle inertia is negligible with respect to the fluid's inertia, particles act as tracers for the fluid motion, and turbulence-induced velocity gradients in the fluid increase collisions (Saffman & Turner, 1956). As particles grow, their inertia becomes comparable to that of eddies on the smallest scales of the flow and particles are subject to so-called inertial effects. Particles tend to cluster in regions of the flow with lower vorticity, and centrifugal forces generated by the eddies enhance relative velocities between particles, leading to large relative velocities even between particles of similar sizes (Shaw et al., 1998; Squires & Eaton, 1991; Voßkuhle et al., 2014). The relevance of these effects for increasing collisions between ice particles, as well as ice particles and supercooled droplets has been suggested by Naso et al. (2018) and Sheikh et al. (2022), among others.

To our knowledge, these theoretical considerations have been poorly supported by observations in atmospheric clouds. Based on case studies, a handful of authors have identified shear layers as regions of precipitation enhancement in orographic precipitation (Aikins et al., 2016; Gehring et al., 2022; Grazioli et al., 2015; Houze & Medina, 2005; Medina & Houze, 2015; Ramelli et al., 2021) and in warm conveyor belts (Gehring et al., 2020). Out of the mentioned studies, Houze and Medina (2005) first suggested that shear leads to the formation of overturning cells, and that subcellular motions might favor increasing differential settling velocities between hydrometeors, leading to enhanced aggregation and riming. Recently, Fitch and Garrett (2022b) reported that in Arctic low-level mixed-phase clouds graupel settling velocity and density increase with increasing turbulence.

Here, we present a new view on the subject of ice growth enhancement by turbulence, investigating the topic in low-level mixed-phase clouds (LLMPCs) at the Arctic site of Ny-Ålesund. Arctic LLMPCs are inherently turbulent, as the liquid layer, typically located close to cloud top, drives radiative cooling, which in turn produces buoyant overturning and turbulence throughout the cloud layer (e.g., Morrison et al., 2012). Ice is nucleated and grows in the liquid layer, first by vapor deposition, then via collisional processes, both by riming (Fitch & Garrett, 2022a; Maherndl et al., 2024), and by aggregation (Chellini et al., 2022). It is in the liquid layer that subcellular turbulent motions could potentially increase the collision rates between cloud particles, leading to an enhancement in aggregation and riming. Due to the limited depth of LLMPCs, information on cloud top temperature (CTT) allows us to constrain the ice habits that are nucleated (Bühl et al., 2016; Myagkov et al., 2016). Furthermore, the wide range of liquid water path (LWP) values typically observed, from a few tens up to 400 g m^{-2} (Chellini et al., 2022; Gierens et al., 2020), allows us to discriminate between scenarios with varying likelihood of riming. Hence, the wide spectrum of conditions provided by Arctic LLMPCs makes them ideal natural laboratories to test the dependence of the turbulence-ice-growth interaction on ice habits and varying supercooled liquid availability conditions.

2. Methods

We use the long-term data set of ground-based remote-sensing observations presented in Chellini et al. (2023b), which includes dual-wavelength and polarimetric Doppler cloud radar observations, as well as thermodynamic retrievals from a microwave radiometer. Millimeter-wavelength cloud radars have been widely used to study Arctic cloud properties and processes (e.g., Griesche et al., 2021; Kalesse et al., 2016; Luke et al., 2021; Shupe et al., 2006; Zhao & Garrett, 2008). Additionally, dual-wavelength and polarimetric observations respectively provide information on ice particle characteristic size and shape (e.g., Bringi & Chandrasekar, 2001; Hogan et al., 2000), and similar data sets have been used in past studies to investigate ice microphysical processes (e.g., Barrett et al., 2019; Dias Neto et al., 2019; Tetoni et al., 2022; Trömel et al., 2021). Doppler observations further provide the unique opportunity to retrieve the EDR (Borque et al., 2016; Bouniol et al., 2004; Rogers & Tripp, 1964), which is the key turbulence variable characterizing small-scale turbulent dynamics, and therefore determining hydrometeor collision rates (Pumir & Wilkinson, 2016; Vaillancourt & Yau, 2000).

The data set was recorded at the AWIPEV observatory in Ny-Ålesund, located on the western coast of Svalbard at 79°N. It spans a 15-month period from 10 October 2021 until 31 December 2022, and only includes LLMPC events. The events were selected by requiring that ice and liquid phases, identified with the Cloudnet target classification (Illingworth et al., 2007), coexist for at least 1 hour, and cloud top remains below 2,500 m. The

19448007, 2024, 6, Downloaded from https://agupubs.onlinelibrary.wiley.com/doi/10.1029/2023GL106599 by Bibl. der Universitat zu Koln, Wiley Online Library on [12/11/2026]. See the Terms and Conditions (https://onlinelibrary.wiley.com/terms-and-conditions) on Wiley Online Library for rules of use; OA articles are governed by the applicable Creative Commons License

two cornerstones of the data set are a 94-GHz zenith-pointing single-polarization Doppler radar (hereafter referred to as W-band; Küchler et al., 2017), and a 35-GHz scanning dual-polarization Doppler radar (hereafter Ka-band; Chellini et al., 2023b). The radar data have undergone quality control and post-processing, including attenuation corrections. Temperature profiles and LWP from a co-located microwave radiometer have been retrieved following the approaches by Crewell and Löhnert (2007) and Nomokonova et al. (2020). For further technical details on the data set and the processing methods applied we refer the reader to Chellini et al. (2023b).

We use equivalent radar reflectivity factor (hereafter reflectivity) Z_e and mean Doppler velocity (MDV) observed by the W-band in zenith, while polarimetric variables are taken from Ka-band observations at 30–40° elevation. Zenith reflectivities from the two systems are combined into the dual-wavelength ratio (DWR). The DWR is the ratio (in linear scale) between reflectivities observed at two separate frequencies, and is sensitive to the characteristic size of the ice particle population in the size range where hydrometeor backscattering is in the Rayleigh regime at the lower frequency, and non-Rayleigh at the higher frequency (Battaglia et al., 2020). For the used frequency combination (35–94 GHz), DWR is sensitive to mean particle sizes ranging from 0.5 to 5 mm approximately, and takes on increasing values up to approximately 10 dB, where it saturates and is no longer sensitive to further increases in size (e.g., Ori et al., 2020). As for polarimetric variables, we focus on differential reflectivity Z_{DR}, mostly sensitive to the aspect ratio, density, and size of asymmetrical particles (Griffin et al., 2018; Schrom & Kumjian, 2016), correlation coefficient ρ_{HV}, which decreases with increasing diversity in shape and orientation of particles (Andrić et al., 2013), and specific differential phase K_{DP}, related to the number concentration of small asymmetric ice particles (Bechini et al., 2013; Schrom et al., 2015). The EDR is retrieved via the variance of velocity time series, using a modified version of the approach by Borque et al. (2016). Further details are given in the Supplement.

3. Case Study

Before we present and discuss the statistical analysis based on the long-term LLMPC data set (Section 4), we shortly illustrate the typical structure of LLMPCs occurring over Ny-Ålesund and introduce the most relevant observables in a case study (Figure 1). We can identify three main periods based on turbulence characteristics: a first period from 3:00 until 5:00 UTC, when EDR is below 10^{-4} m^2 s^{-3} throughout the cloud layer, a second period between 5:00 and 11:00 UTC when EDR increases at cloud top, reaching values between 10^{-4} and 10^{-3} m^2 s^{-3}, and a third period after 11:00 UTC when EDR at cloud top is close to or higher than 10^{-3} m^2 s^{-3}, and high EDR values are found also below liquid base. The three periods are accompanied by varying microphysical fingerprints in the radar data.

The first two periods are characterized by similar CTTs close to −13°C and LWP values mostly below 50 g m^{-2}. During the first period of low turbulence at cloud top, we find Z_{DR} values reaching up to 4 dB, consistent with the expected growth of dendritic particles within this temperature regime (e.g., Takahashi, 2014). As soon as turbulence at cloud top increases (ca. 5 UTC), Z_{DR} drops, and DWR below the liquid layer increases to values between 4 and 7 dB. The increase in DWR together with the overall small change in MDV strongly suggests that the increasing turbulence fosters the formation of larger aggregates.

The third period with most intense turbulence seems to favor riming, likely alongside aggregation: DWR increases further up to 8–10 dB, accompanied by MDV exceeding, in some regions, values of 1.5 m s^{-1}, and much higher LWP values ranging between 100 and 350 g m^{-2}. The high MDV values are indicative of higher-density rimed particles (Kneifel & Moisseev, 2020; Mosimann, 1995), whose more spherical shape is consistent with Z_{DR} values being close to 0 dB.

While the case study presented already establishes a potential connection between turbulence and collisional ice-growth processes in LLMPCs, the presence of such interaction can only be demonstrated via robust statistics based on a high number of events. Such analysis is presented in the next section.

4. Results and Discussion

In this section we test the sensitivity of ice growth processes to varying turbulence conditions, discriminating the cases into various classes, based on ice habit (via CTT) and availability of liquid (via LWP). We build upon the results by Chellini et al. (2022), who observed that ice aggregation predominantly occurs in LLMPCs at Ny-

19448007, 2024, 6, Downloaded from https://agupubs.onlinelibrary.wiley.com/doi/10.1029/2023GL106599 by Bibl. der Universitat zu Koln, Wiley Online Library on [12/11/2026]. See the Terms and Conditions (https://onlinelibrary.wiley.com/terms-and-conditions) on Wiley Online Library for rules of use; OA articles are governed by the applicable Creative Commons License

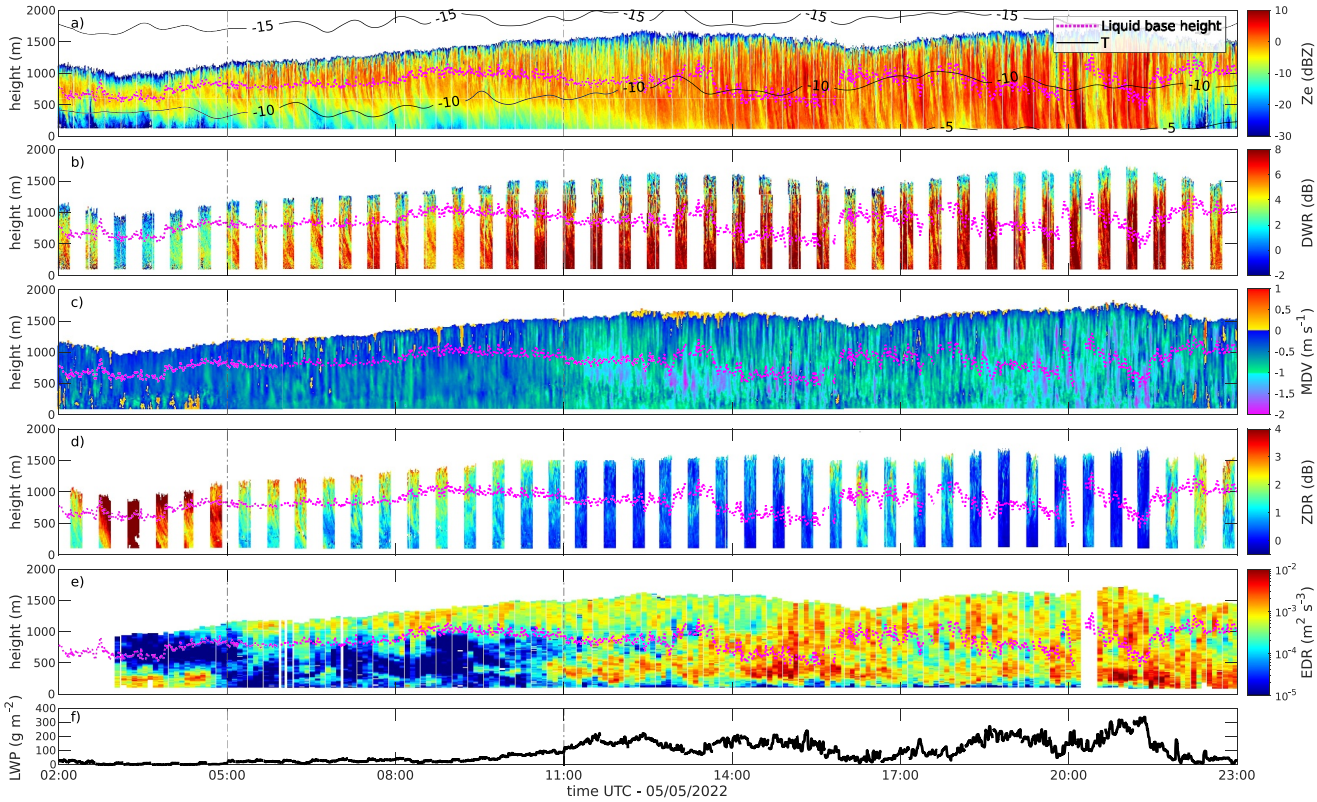


Figure 1. Case study of low-level mixed-phase cloud, detected on 5 May 2022. Panels respectively display: reflectivity from W-band radar with temperature contours overlayed (a), Ka-W dual-wavelength ratio (b), mean Doppler velocity from W-band radar, smoothed with a 2-min rolling average (c; negative values indicate targets moving toward the radar), differential reflectivity from Ka-band observations at 30° elevation (d), eddy dissipation rate (e), liquid water path (f). The dotted magenta line on panels a through e indicates liquid base height from a ceilometer, while the contours in panel a indicate temperature in °C retrieved from microwave radiometer data. Vertical dash-dotted lines indicate the three periods identified in the text.

Ålesund if the liquid layer of the cloud is at temperatures compatible with growth of plate-like particles, that is, between −20 and −10°C. They attributed this to the rapid growth of dendritic particles, favored by saturation with respect to liquid; dendrites then aggregate efficiently due to their large cross sectional area and sticking efficiency (Pruppacher & Klett, 2012). Chellini et al. (2022) then reported a dramatic decrease in occurrence of ice aggregates when CTT is warmer than −10°C, hence the production of large, fast-falling particles in this temperature regime can be predominantly explained by riming. Therefore, we here classify all available profiles into either a *dendritic-growth regime* (CTT between −20 and −10°C), where both aggregation and riming can occur, or a *columnar regime* (CTT between −10 and −2°C), where predominantly riming can take place. In order to determine connections between microphysics and turbulence we classify profiles based on the mean EDR calculated across the layer between cloud top and 500 m below cloud top (or subsets thereof in case of thinner clouds). The mean is computed in log-scale, as EDR is typically thought to be log-normally distributed (e.g., Siebert et al., 2006). The reasoning behind this approach is given in the Supplement, together with distributions of uppermost-500-m averaged EDR. All available profiles are classified into three EDR classes: EDR < 10^{-4} m^2 s^{-3}, EDR between 10^{-4} and 10^{-3} m^2 s^{-3}, and EDR > 10^{-3} m^2 s^{-3}. They were determined based on the quartiles of the distribution of uppermost-500-m averaged EDR throughout all events, which are: $10^{-4.2}$, $10^{-3.5}$, $10^{-2.9}$ m^2 s^{-3}. The number of samples available in each CTT and EDR class is given in the Supplement.

4.1. Dependence of Radar Observables on EDR

The signatures obtained in the dendritic-growth regime in Figures 2a–2f confirm that the main ice-growth process in this temperature regime is aggregation. All median curves display values close to 0.6–0.7 m s^{-1}, compatible with low-density aggregates (Karrer et al., 2020; Locatelli & Hobbs, 1974). Increasing DWR with increasing EDR in Figure 2b suggests that aggregation might be indeed enhanced by higher EDR. The three median DWR

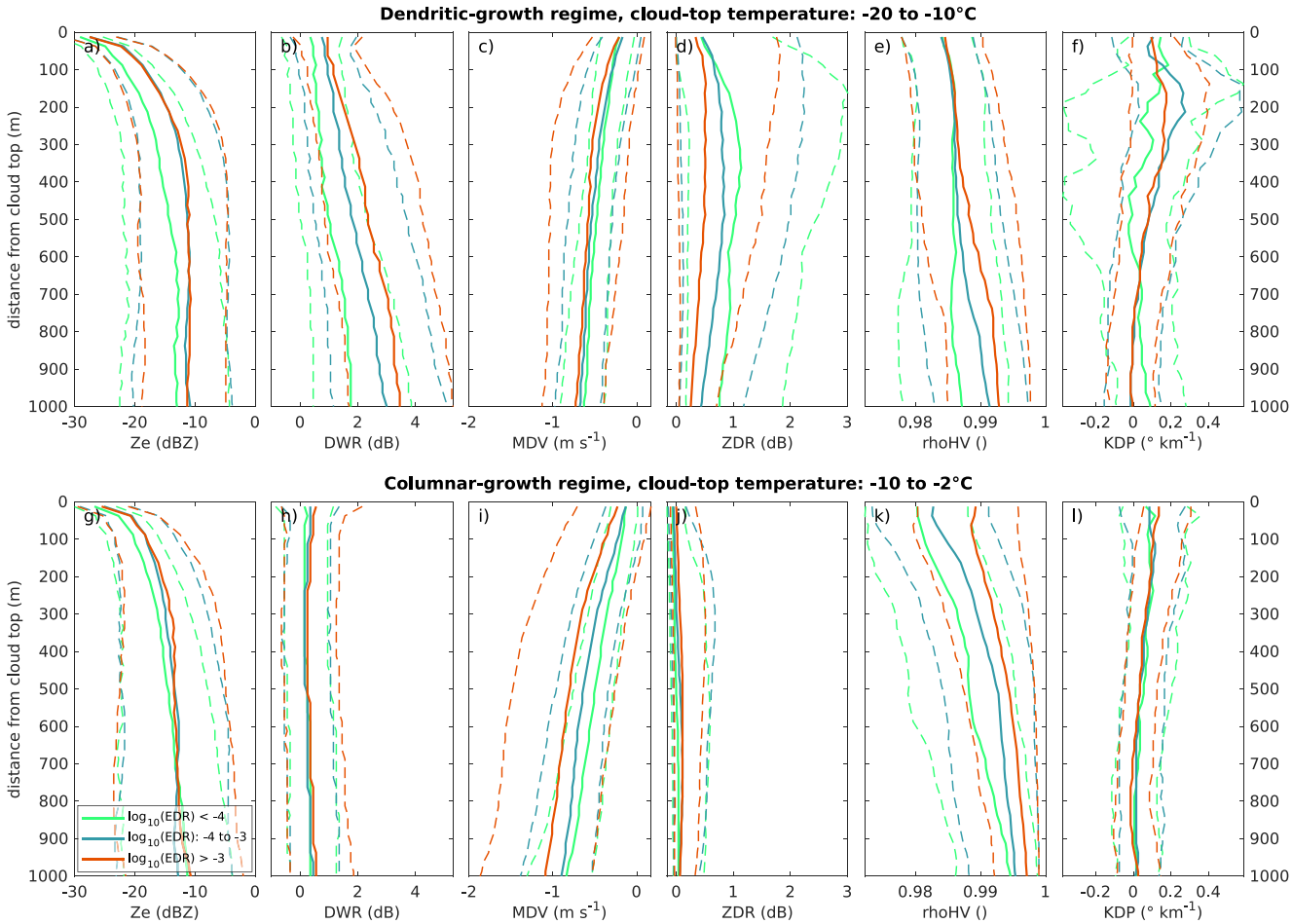


Figure 2. Contoured frequency by altitude diagram of several radar variables in eddy dissipation rate (EDR) classes, for profiles with cloud top temperature between −20 and −10°C (a–f) and between −10 and −2°C (g–l). Solid lines indicate median values, dashed lines indicate lower and upper quartiles. Panels respectively display: reflectivity from W-band radar (a, g), Ka-W dual-wavelength ratio (b, h), mean Doppler velocity from W-band radar (c, i), differential reflectivity (d, j), correlation coefficient (e, k), specific differential phase (f, l). The *y*-axis indicates the distance from cloud top along the vertical direction. Profiles are classified based on the mean EDR across the topmost 500 m of the cloud layer. EDR values in the legend are reported in $m^2\ s^{-3}$, height bins are 25 m wide.

curves especially diverge in the top 500 m, with median values at 500 m below cloud top of 1.0, 1.8, and 2.4 dB. Z_{DR} in the low EDR class displays a vastly different behavior compared to the intermediate and high EDR classes: it increases from cloud top until 300–400 m below cloud top, then decreases. This could be a signature of depositional growth. The absence of such signature in the two remaining EDR classes likely originates from onsetting aggregation already close to cloud top. Similar features were already observed when comparing the first and second period in the case study in Figure 1. Hence, we argue that the combined decrease in Z_{DR} and increase in DWR with EDR and height are a clear indication of increasing aggregation with turbulence.

In the classical theory of aggregation, the process is considered one-dimensional, taking place along the vertical axis, and driven by sedimentation velocity differences (e.g., Field & Heymsfield, 2003; Westbrook et al., 2004). Turbulence can strongly enhance relative velocities both in the vertical and horizontal components and also lead to locally enhanced particle concentrations. Direct numerical simulations by Sheikh et al. (2022) with 300-μm plate particles revealed that collision kernels display an approximate power law dependence on EDR with exponent 0.5. In the case of inertial particles, they attributed the collision rate increases to enhanced relative velocities generated by centrifugal forces. The lack of a clear peak in Z_{DR} in the intermediate and high EDR cases in Figure 2d, compared to the low EDR, suggests that such an enhancement in collision rate might already be relevant close to cloud top. The enhanced K_{DP} between 100 and 300 m below cloud top might also be a consequence of an increase in collision rates, as it signals a higher number concentration of small particles. One possible explanation for this signature might be fragmentation of dendritic and stellar structures during particle

19448007, 2024, 6, Downloaded from https://agupubs.onlinelibrary.wiley.com/doi/10.1029/2023GL106599 by Bibl. der Universitat zu Koln, Wiley Online Library on [12/11/2026]. See the Terms and Conditions (https://onlinelibrary.wiley.com/terms-and-conditions) on Wiley Online Library for rules of use; OA articles are governed by the applicable Creative Commons License

19448007, 2024, 6, Downloaded from https://agupubs.onlinelibrary.wiley.com/doi/10.1029/2023GL106599 by Bibl. der Universitat zu Koln, Wiley Online Library on [12/11/2026]. See the Terms and Conditions (https://onlinelibrary.wiley.com/terms-and-conditions) on Wiley Online Library for rules of use; OA articles are governed by the applicable Creative Commons License

collisions, which has been frequently suggested in literature (e.g., Rangno & Hobbs, 2001; Schwarzenboeck et al., 2009; von Terzi et al., 2022).

In the columnar regime, when CTT is higher than −10°C, aggregation is not dominant in our data set, as evident from DWR for the most part being below 1 dB in Figure 2h. Hence, the main relevant ice-growth process is riming: MDV values in panel c are in fact compatible with small high-density ice particles (Barthazy & Schefold, 2006; Locatelli & Hobbs, 1974), and Z_{DR} is close to 0 dB, indicative of the presence of spherical particles. Reflectivity and MDV both display increasing median and quartile values with increasing EDR, while ρ_{HV} displays values reaching closer to unity as particles sediment, and moving from the lower EDR to the higher EDR class. All these signatures are compatible with increasing riming with EDR, however, it cannot be clearly inferred from Figures 2g–2l whether these fingerprints are generated by increased ice-liquid collision rates associated with increasing EDR, or by increased liquid production associated with conditions that favor high EDR. In the next section we disentangle the effects of increased liquid production and turbulence on the ice microphysics.

In Figure 2l K_{DP} displays a similar behavior in all EDR classes, with a maximum at cloud top close to 0.1° km^{-1}, then decreasing with height as particles sediment. Luke et al. (2021) reported the occurrence of secondary ice production in less than 10% of cases of MPCs in this temperature regime at the Arctic site of Utqiaġvik. Assuming a similar frequency of occurrence of secondary ice production at Ny-Ålesund, we can attribute most of the K_{DP} signal in Figure 2l to primary ice production. The maximum at cloud top is likely associated with higher liquid water content (LWC) at cloud top (Mioche et al., 2017), as in Arctic MPCs ice nucleation is thought to originate from the liquid phase (De Boer et al., 2011; Prenni et al., 2009). Assuming that similar primary ice nucleation pathways are present above and below −10°C, the K_{DP} maxima between 100 and 300 m below cloud top in the dendritic regime in Figure 2f can be indeed interpreted as generated by turbulence-induced secondary ice production. Therefore, increasing collision rates with turbulence might lead to higher number of fragments produced by collisions between plate-like particles. However, we do not have an explanation for the higher values of K_{DP} found in the intermediate EDR class compared to those in the high EDR class.

4.2. Combined Impact of LWP and EDR on Riming

In this section we aim at disentangling the contributions from turbulence and LWP, as in LLMPCs higher LWC has been reported in updrafts (Khain et al., 2022; Shupe et al., 2008), and stronger updrafts might in turn be associated with higher EDR. In Figure 3 we display distributions of Z_e and MDV, taken at 500 m below cloud top, classified based on LWP and uppermost-500-m averaged EDR, in the columnar regime. A similar figure for the dendritic regime can be found in the Supplement.

As already mentioned, in this temperature regime we can assume that riming is the dominant ice growth process. Z_e and MDV display an increase with EDR in all LWP classes with LWP > 100 g m^{-2}. The increase in MDV being accompanied by an increase in reflectivity indicates an enhancement in riming. Looking only at the lowest EDR class, median Z_e and MDV remain approximately constant at any LWP value higher than 50 g m^{-2}. Even in the higher LWP classes (LWP > 200 g m^{-2}), the values of Z_e and MDV shown in Figure 3 suggest low degrees of riming when EDR < 10^{-4} m^2 s^{-3}. We argue that this is a strong indication that turbulence is an essential component needed to obtain riming, at least in the shallow liquid layers subject of this study. Furthermore, the increase in interquartile range of the MDV distributions as EDR increases might be attributable, in addition to the intrinsic increase in variance of air velocity associated with higher EDR, to the inhomogeneity of the riming process, which leads to a larger spread in the fall velocity distribution (e.g., Vogl et al., 2022). In the two lowest LWP classes (i.e., LWP < 100 g m^{-2}), reflectivities are similar across all EDR classes, while MDV increases with EDR. This might in part be attributable to settling velocity enhancement by turbulence, via a process known as preferential sweeping (Aliseda et al., 2002; Li et al., 2021; Maxey, 1987).

The riming intensification here reported might be attributed to higher EDR favoring the formation of larger droplets, via collision-coalescence enhancement; riming has been in fact shown to be sensitive to droplet size (Erfani & Mitchell, 2017; Jensen & Harrington, 2015). Erfani and Mitchell (2017) reported that for LWC of 0.05 g m^{-3} a doubling of the mass-median diameter of droplets from 8 to 16 μm quadruples the riming rate. In warm rain formation, the role of turbulence in favoring the formation of collision-coalescence initiators has been suggested. These are droplets sufficiently large to initiate precipitation formation, and are thought to be generated by cloud top turbulence, which locally enhances collision-coalescence (Small & Chuang, 2008). Similarly, in MPCs turbulence might favor the initial formation of rimed crystals, which then collect droplets more and more

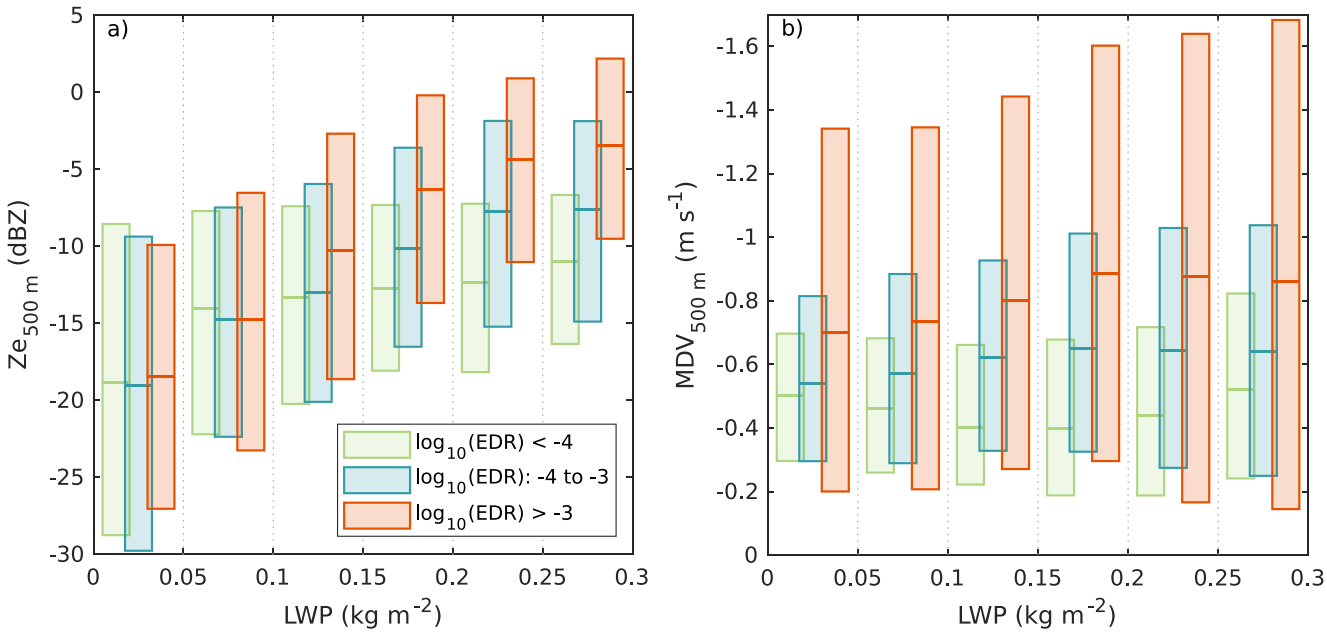


Figure 3. Quartiles of W-band reflectivity (a), and W-band mean Doppler velocity (b), measured at 500 m below cloud top, classified into liquid water path (LWP) and eddy dissipation rate (EDR) classes, for profiles with cloud top temperature between −10 and −2°C. The edges of the LWP classes are indicated on the *x*-axis. Distributions belonging to the same LWP class, but different EDR classes are shifted with respect to each other to facilitate the interpretation of the plot. Profiles are classified based on the mean EDR across the topmost 500 m of the cloud layer. EDR values in the legend are reported in $m^2\ s^{-3}$.

efficiently as they rime, due to the dramatic dependence of collection efficiency on the particle's Reynolds number Re, which in turn increases with size (Wang & Ji, 2000).

In addition to a collision-coalescence enhancement, inertial effects have also been suggested to play a role in the enhancement of ice-liquid collision rates (Pinsky & Khain, 1998). Furthermore, we speculate that turbulence might favor collisions between ice crystals and droplets on the smaller side of the size distribution. Due to the small sizes and relatively low inertia of droplets, modifications of the flow field by the ice particle play a large role in riming. Direct numerical simulation studies have shown that if modifications of the flow by the collector are neglected, collision rates between ice crystals and droplets are only marginally increased under increasing EDR (Naso et al., 2018). In contrast, if the two-way interaction between the collector and the flow is taken into account, an increase in collision efficiency for small particles with EDR at constant collector Re has been suggested by Homann et al. (2016), although they did not investigate cloud microphysics applications specifically.

5. Conclusions

In this study, we use state-of-the-art dual-frequency and polarimetric Doppler cloud radar observations of Arctic low-level mixed-phase clouds to evaluate the role of turbulence in the growth of precipitating ice particles. We perform a statistical analysis based on a large number of events (for a total duration of 3,426 hr), which highlights the key role that turbulence plays in cold precipitation formation. In particular, following previous studies, categorizing the events based on CTT allows us to discriminate between cases where both aggregation and riming are relevant growth processes (at CTT between −20 and −10°C, i.e., at dendritic-growth temperatures), and cases where mainly riming is relevant (at CTT warmer than −10°C, i.e., at columnar-growth temperatures). The main findings of this study are as follows:

- At dendritic-growth temperatures, higher EDR is associated with increasing size of ice particles. We argue that such an increase is attributable to increasing collision rates between ice particles, leading to larger aggregates. We suggest that, in this temperature regime, increasing collision rates with EDR might lead to increasing secondary ice production via fragmentation of dendritic structures, in addition to an enhancement in aggregation.

19448007, 2024, 6, Downloaded from https://agupubs.onlinelibrary.wiley.com/doi/10.1029/2023GL106599 by Bibl. der Universitat zu Koln, Wiley Online Library on [12/11/2026]. See the Terms and Conditions (https://onlinelibrary.wiley.com/terms-and-conditions) on Wiley Online Library for rules of use; OA articles are governed by the applicable Creative Commons License

19448007, 2024, 6, Downloaded from https://agupubs.onlinelibrary.wiley.com/doi/10.1029/2023GL106599 by Bibl. der Universitat zu Koln, Wiley Online Library on [12/11/2026]. See the Terms and Conditions (https://onlinelibrary.wiley.com/terms-and-conditions) on Wiley Online Library for rules of use; OA articles are governed by the applicable Creative Commons License

- At temperatures warmer than −10°C, turbulence appears to increase riming rates. Dramatic increases in MDV and reflectivity (up to 120% in MDV and 8 dB in Z_e) with increasing EDR and constant LWP are observed, suggesting that riming in shallow liquid layers, such as those observed in the LLMPCs here studied, is a fundamentally turbulent process. We discuss a number of possible processes that could lead to the observed increased riming rates, however the remote sensing observations here used do not allow us either to pinpoint or exclude specific processes. We deem that further work combining model experiments with remote-sensing observations is highly needed in this regard to explain the riming rate enhancement here reported.

We argue that turbulence is potentially a key component determining the characteristics of precipitation. The current study only highlighted this key role in shallow clouds characterized by low to intermediate EDR values, between 10^{-5} and 10^{-2} m^2 s^{-3}. Mid-latitude frontal systems display similar values (Chapman & Browning, 2001), while deep convective systems have been reported to produce EDR up to $10^{-0.5}$ m^2 s^{-3} (Feist et al., 2019). Therefore interactions between turbulence and ice growth might be at play in many cloud systems that produce precipitation at mid-latitudes. The inclusion of turbulence-dependent collision kernels for collision-coalescence has been shown to produce large improvements in warm rain formation in models (e.g., Seifert et al., 2010). We thus argue that fully quantifying and parametrizing the impact of turbulence on snow and graupel growth is crucial to improve model performance. The development of such parametrizations will need to rely on coincident remote-sensing and in-situ observations (either air- or balloon-borne), as the latter would allow for an accurate quantification of aggregate characteristics and rime mass fraction. Furthermore, large efforts are needed to reach a theoretical understanding of particle inertial effects in snow, as well as the processes leading to riming enhancement in turbulence.

Data Availability Statement

The remote-sensing data used in this study have been published in Chellini et al. (2023a), and are described in Chellini et al. (2023b). The slow edge velocity, needed as input for the EDR retrieval, together with the EDR retrieval output, have been published separately in Chellini (2023).

Acknowledgments
The authors gratefully acknowledge the funding by the Deutsche Forschungsgemeinschaft (DFG, German Research Foundation)–project no. 268020496–TRR 172, within the Transregional Collaborative Research Center "ArctiC Amplification: Climate Relevant Atmospheric and SurfaCe Processes, and Feedback Mechanisms $(AC)^3$". The authors would like to express their gratitude to Paloma Borque and Rosa Gierens, for sharing code used in the EDR retrieval, and to Sabrina Schnitt, for providing detailed feedback on the manuscript. The authors would like to further acknowledge discussions with Eberhard Bodenschatz, Ulrich Löhnert, Maximilian Mahan, Dmitri Moisseev, Axel Seifert, Raymond Shaw, Christoph Siewert, and Miklós Szakáll, among others, whose constructive comments and criticism helped shape the analysis. The authors would like to express their gratitude to the two anonymous reviewers, whose constructive criticism helped improve the quality of the manuscript. GC further acknowledges the support from the Graduate School of Geosciences (GSGS) of the University of Cologne, and the Integrated Research Training group (IRTG) of the $(AC)^3$ consortium. Open Access funding enabled and organized by Projekt DEAL.

References

Aikins, J., Friedrich, K., Geerts, B., & Pokharel, B. (2016). Role of a cross-barrier jet and turbulence on winter orographic snowfall. *Monthly Weather Review*, *144*(9), 3277–3300. https://doi.org/10.1175/MWR-D-16-0025.1

Aliseda, A., Cartellier, A., Hainaux, F., & Lasheras, J. C. (2002). Effect of preferential concentration on the settling velocity of heavy particles in homogeneous isotropic turbulence. *Journal of Fluid Mechanics*, *468*, 77–105. https://doi.org/10.1017/S0022112002001593

Andrić, J., Kumjian, M. R., Zrnić, D. S., Straka, J. M., & Melnikov, V. M. (2013). Polarimetric signatures above the melting layer in winter storms: An observational and modeling study. *Journal of Applied Meteorology and Climatology*, *52*(3), 682–700. https://doi.org/10.1175/JAMC-D-12-028.1

Arenberg, D. (1939). Turbulence as the major factor in the growth of cloud drops. *Bulletin of the American Meteorological Society*, *20*(10), 444–448. https://doi.org/10.1175/1520-0477-20.10.444

Barrett, A. I., Westbrook, C. D., Nicol, J. C., & Stein, T. H. M. (2019). Rapid ice aggregation process revealed through triple-wavelength Doppler spectrum radar analysis. *Atmospheric Chemistry and Physics*, *19*(8), 5753–5769. https://doi.org/10.5194/acp-19-5753-2019

Barthazy, E., & Schefold, R. (2006). Fall velocity of snowflakes of different riming degree and crystal types. *Atmospheric Research*, *82*(1–2), 391–398. https://doi.org/10.1016/j.atmosres.2005.12.009

Battaglia, A., Tanelli, S., Tridon, F., Kneifel, S., Leinonen, J., & Kollias, P. (2020). Triple-frequency radar retrievals. In V. Levizzani, C. Kidd, D. B. Kirschbaum, C. D. Kummerow, K. Nakamura, & F. J. Turk (Eds.), *Satellite precipitation measurement* (Vol. 1, pp. 211–229). Springer International Publishing. https://doi.org/10.1007/978-3-030-24568-9_13

Bechini, R., Baldini, L., & Chandrasekar, V. (2013). Polarimetric radar observations in the ice region of precipitating clouds at C-band and X-band radar frequencies. *Journal of Applied Meteorology and Climatology*, *52*(5), 1147–1169. https://doi.org/10.1175/JAMC-D-12-055.1

Billault-Roux, A.-C., Georgakaki, P., Gehring, J., Jaffeux, L., Schwarzenboeck, A., Coutris, P., et al. (2023). Distinct secondary ice production processes observed in radar Doppler spectra: Insights from a case study. *Atmospheric Chemistry and Physics*, *23*(17), 10207–10234. https://doi.org/10.5194/acp-23-10207-2023

Borque, P., Luke, E., & Kollias, P. (2016). On the unified estimation of turbulence eddy dissipation rate using Doppler cloud radars and lidars. *Journal of Geophysical Research: Atmospheres*, *121*(10), 5972–5989. https://doi.org/10.1002/2015JD024543

Bouniol, D., Illingworth, A., & Hogan, R. (2004). Deriving turbulent kinetic energy dissipation rate within clouds using ground based radar. *Proceedings of ERAD*, *281*.

Bringi, V. N., & Chandrasekar, V. (2001). *Polarimetric Doppler weather radar: Principles and applications*. Cambridge University Press.

Bühl, J., Seifert, P., Myagkov, A., & Ansmann, A. (2016). Measuring ice-and liquid-water properties in mixed-phase cloud layers at the Leipzig Cloudnet station. *Atmospheric Chemistry and Physics*, *16*(16), 10609–10620. https://doi.org/10.5194/acp-16-10609-2016

Chapman, D., & Browning, K. (2001). Measurements of dissipation rate in frontal zones. *Quarterly Journal of the Royal Meteorological Society*, *127*(576), 1939–1959. https://doi.org/10.1002/qj.49712757605

Chellini, G. (2023). Supplement to "Low-level mixed-phase clouds at the high Arctic site of Ny-Ålesund: A comprehensive long-term dataset of remote sensing observations" [Dataset]. *Zenodo*. https://doi.org/10.5281/zenodo.8325221

Chellini, G., Gierens, R., Ebell, K., Kiszler, T., & Kneifel, S. (2023a). Low-level mixed-phase clouds at the high Arctic site of Ny-Ålesund: A comprehensive long-term dataset of remote sensing observations [Dataset]. *Zenodo*. https://doi.org/10.5281/zenodo.7803064

Chellini, G., Gierens, R., Ebell, K., Kiszler, T., Krobot, P., Myagkov, A., et al. (2023b). Low-level mixed-phase clouds at the high Arctic site of Ny-Ålesund: A comprehensive long-term dataset of remote sensing observations. *Earth System Science Data*, *15*(12), 5427–5448. https://doi.org/10.5194/essd-15-5427-2023

Chellini, G., Gierens, R., & Kneifel, S. (2022). Ice aggregation in low-level mixed-phase clouds at a high Arctic site: Enhanced by dendritic growth and absent close to the melting level. *Journal of Geophysical Research: Atmospheres*, *127*(16), e2022JD036860. https://doi.org/10.1029/2022JD036860

Crewell, S., & Löhnert, U. (2007). Accuracy of boundary layer temperature profiles retrieved with multifrequency multiangle microwave radiometry. *IEEE Transactions on Geoscience and Remote Sensing*, *45*(7), 2195–2201. https://doi.org/10.1109/TGRS.2006.888434

De Boer, G., Morrison, H., Shupe, M., & Hildner, R. (2011). Evidence of liquid dependent ice nucleation in high-latitude stratiform clouds from surface remote sensors. *Geophysical Research Letters*, *38*(1). https://doi.org/10.1029/2010GL046016

Dias Neto, J., Kneifel, S., Ori, D., Trömel, S., Handwerker, J., Bohn, B., et al. (2019). The TRIple-frequency and Polarimetric radar Experiment for improving process observations of winter precipitation. *Earth System Science Data*, *11*(2), 845–863. https://doi.org/10.5194/essd-11-845-2019

East, T. W. R., & Marshall, J. (1954). Turbulence in clouds as a factor in precipitation. *Quarterly Journal of the Royal Meteorological Society*, *80*(343), 26–47. https://doi.org/10.1002/qj.49708034305

Erfani, E., & Mitchell, D. L. (2017). Growth of ice particle mass and projected area during riming. *Atmospheric Chemistry and Physics*, *17*(2), 1241–1257. https://doi.org/10.5194/acp-17-1241-2017

Feist, M. M., Westbrook, C. D., Clark, P. A., Stein, T. H., Lean, H. W., & Stirling, A. J. (2019). Statistics of convective cloud turbulence from a comprehensive turbulence retrieval method for radar observations. *Quarterly Journal of the Royal Meteorological Society*, *145*(719), 727–744. https://doi.org/10.1002/qj.3462

Field, P. R., & Heymsfield, A. J. (2003). Aggregation and scaling of ice crystal size distributions. *Journal of the Atmospheric Sciences*, *60*(3), 544–560. https://doi.org/10.1175/1520-0469(2003)060⟨0544:AASOIC⟩2.0.CO;2

Fitch, K. E., & Garrett, T. J. (2022a). Graupel precipitating from thin Arctic clouds with liquid water paths less than 50 g m-2. *Geophysical Research Letters*, *49*(1), e2021GL094075. https://doi.org/10.1029/2021GL094075

Fitch, K. E., & Garrett, T. J. (2022b). Measurement and analysis of the microphysical properties of Arctic precipitation showing frequent occurrence of riming. *Journal of Geophysical Research: Atmospheres*, *127*(7), e2021JD035980. https://doi.org/10.1029/2021JD035980

Gehring, J., Oertel, A., Vignon, É., Jullien, N., Besic, N., & Berne, A. (2020). Microphysics and dynamics of snowfall associated with a warm conveyor belt over Korea. *Atmospheric Chemistry and Physics*, *20*(12), 7373–7392. https://doi.org/10.5194/acp-20-7373-2020

Gehring, J., Vignon, É., Billault-Roux, A.-C., Ferrone, A., Protat, A., Alexander, S. P., & Berne, A. (2022). Orographic flow influence on precipitation during an atmospheric river event at Davis, Antarctica. *Journal of Geophysical Research: Atmospheres*, *127*(2), e2021JD035210. https://doi.org/10.1029/2021JD035210

Gierens, R., Kneifel, S., Shupe, M. D., Ebell, K., Maturilli, M., & Löhnert, U. (2020). Low-level mixed-phase clouds in a complex Arctic environment. *Atmospheric Chemistry and Physics*, *20*(6), 3459–3481. https://doi.org/10.5194/acp-20-3459-2020

Grazioli, J., Lloyd, G., Panziera, L., Hoyle, C. R., Connolly, P. J., Henneberger, J., & Berne, A. (2015). Polarimetric radar and in situ observations of riming and snowfall microphysics during CLACE 2014. *Atmospheric Chemistry and Physics*, *15*(23), 13787–13802. https://doi.org/10.5194/acp-15-13787-2015

Griesche, H. J., Ohneiser, K., Seifert, P., Radenz, M., Engelmann, R., & Ansmann, A. (2021). Contrasting ice formation in Arctic clouds: Surface-coupled vs. surface-decoupled clouds. *Atmospheric Chemistry and Physics*, *21*(13), 10357–10374. https://doi.org/10.5194/acp-21-10357-2021

Griffin, E. M., Schuur, T. J., & Ryzhkov, A. V. (2018). A polarimetric analysis of ice microphysical processes in snow, using quasi-vertical profiles. *Journal of Applied Meteorology and Climatology*, *57*(1), 31–50. https://doi.org/10.1175/JAMC-D-17-0033.1

Heymsfield, A. J., Schmitt, C., Bansemer, A., Gettelman, A., Field, P. R., Liu, C., et al. (2020). Contributions of the liquid and ice phases to global surface precipitation: Observations and global climate modeling. *Journal of the Atmospheric Sciences*, *77*(8), 2629–2648. https://doi.org/10.1175/JAS-D-19-0352.1

Hogan, R. J., Illingworth, A. J., & Sauvageot, H. (2000). Measuring crystal size in cirrus using 35-and 94-GHz radars. *Journal of Atmospheric and Oceanic Technology*, *17*(1), 27–37. https://doi.org/10.1175/1520-0426(2000)017⟨0027:MCSICU⟩2.0.CO;2

Homann, H., Guillot, T., Bec, J., Ormel, C., Ida, S., & Tanga, P. (2016). Effect of turbulence on collisions of dust particles with planetesimals in protoplanetary disks. *Astronomy and Astrophysics*, *589*, A129. https://doi.org/10.1051/0004-6361/201527344

Houze, R. A., & Medina, S. (2005). Turbulence as a mechanism for orographic precipitation enhancement. *Journal of the Atmospheric Sciences*, *62*(10), 3599–3623. https://doi.org/10.1175/JAS3555.1

Illingworth, A., Hogan, R., O'connor, E., Bouniol, D., Brooks, M., Delanoë, J., et al., (2007). Cloudnet: Continuous evaluation of cloud profiles in seven operational models using ground-based observations. *Bulletin of the American Meteorological Society*, *88*(6), 883–898. https://doi.org/10.1175/bams-88-6-883

Jensen, A. A., & Harrington, J. Y. (2015). Modeling ice crystal aspect ratio evolution during riming: A single-particle growth model. *Journal of the Atmospheric Sciences*, *72*(7), 2569–2590. https://doi.org/10.1175/JAS-D-14-0297.1

Kalesse, H., de Boer, G., Solomon, A., Oue, M., Ahlgrimm, M., Zhang, D., et al. (2016). Understanding rapid changes in phase partitioning between cloud liquid and ice in stratiform mixed-phase clouds: An Arctic case study. *Monthly Weather Review*, *144*(12), 4805–4826. https://doi.org/10.1175/MWR-D-16-0155.1

Karrer, M., Seifert, A., Siewert, C., Ori, D., von Lerber, A., & Kneifel, S. (2020). Ice particle properties inferred from aggregation modelling. *Journal of Advances in Modeling Earth Systems*, *12*(8), e2020MS002066. https://doi.org/10.1029/2020MS002066

Khain, A., Pinsky, M., & Korolev, A. (2022). Combined effect of the Wegener–Bergeron–Findeisen mechanism and large eddies on microphysics of mixed-phase stratiform clouds. *Journal of the Atmospheric Sciences*, *79*(2), 383–407. https://doi.org/10.1175/JAS-D-20-0269.1

Kneifel, S., & Moisseev, D. (2020). Long-term statistics of riming in nonconvective clouds derived from ground-based Doppler cloud radar observations. *Journal of the Atmospheric Sciences*, *77*(10), 3495–3508. https://doi.org/10.1175/JAS-D-20-0007.1

Küchler, N., Kneifel, S., Löhnert, U., Kollias, P., Czekala, H., & Rose, T. (2017). A W-band radar–radiometer system for accurate and continuous monitoring of clouds and precipitation. *Journal of Atmospheric and Oceanic Technology*, *34*(11), 2375–2392. https://doi.org/10.1175/JTECH-D-17-0019.1

Li, J., Abraham, A., Guala, M., & Hong, J. (2021). Evidence of preferential sweeping during snow settling in atmospheric turbulence. *Journal of Fluid Mechanics*, *928*, A8. https://doi.org/10.1017/jfm.2021.816

Locatelli, J. D., & Hobbs, P. V. (1974). Fall speeds and masses of solid precipitation particles. *Journal of Geophysical Research*, *79*(15), 2185–2197. https://doi.org/10.1029/JC079i015p02185

Luke, E. P., Yang, F., Kollias, P., Vogelmann, A. M., & Maahn, M. (2021). New insights into ice multiplication using remote-sensing observations of slightly supercooled mixed-phase clouds in the Arctic. *Proceedings of the National Academy of Sciences*, *118*(13). https://doi.org/10.1073/pnas.2021387118

19448007, 2024, 6, Downloaded from https://agupubs.onlinelibrary.wiley.com/doi/10.1029/2023GL106599 by Bibl. der Universitat zu Koln, Wiley Online Library on [12/11/2026]. See the Terms and Conditions (https://onlinelibrary.wiley.com/terms-and-conditions) on Wiley Online Library for rules of use; OA articles are governed by the applicable Creative Commons License

Maherndl, N., Moser, M., Lucke, J., Mech, M., Risse, N., Schirmacher, I., & Maahn, M. (2024). Quantifying riming from airborne data during the HALO-(AC)^3 campaign. *Atmospheric Measurement Techniques*, *17*, 1475–1495. https://doi.org/10.5194/amt-17-1475-2024

Maxey, M. R. (1987). The gravitational settling of aerosol particles in homogeneous turbulence and random flow fields. *Journal of Fluid Mechanics*, *174*, 441–465. https://doi.org/10.1017/S0022112087000193

Medina, S., & Houze, R. A. (2015). Small-scale precipitation elements in midlatitude cyclones crossing the California Sierra Nevada. *Monthly Weather Review*, *143*(7), 2842–2870. https://doi.org/10.1175/MWR-D-14-00124.1

Mioche, G., Jourdan, O., Delanoë, J., Gourbeyre, C., Febvre, G., Dupuy, R., et al. (2017). Vertical distribution of microphysical properties of Arctic springtime low-level mixed-phase clouds over the Greenland and Norwegian seas. *Atmospheric Chemistry and Physics*, *17*(20), 12845–12869. https://doi.org/10.5194/acp-17-12845-2017

Morrison, H., de Boer, G., Feingold, G., Harrington, J., Shupe, M. D., & Sulia, K. (2012). Resilience of persistent Arctic mixed-phase clouds. *Nature Geoscience*, *5*(1), 11–17. https://doi.org/10.1038/ngeo1332

Mosimann, L. (1995). An improved method for determining the degree of snow crystal riming by vertical Doppler radar. *Atmospheric Research*, *37*(4), 305–323. https://doi.org/10.1016/0169-8095(94)00050-N

Mülmenstädt, J., Sourdeval, O., Delanoë, J., & Quaas, J. (2015). Frequency of occurrence of rain from liquid-mixed-and ice-phase clouds derived from A-Train satellite retrievals. *Geophysical Research Letters*, *42*(15), 6502–6509. https://doi.org/10.1002/2015GL064604

Myagkov, A., Seifert, P., Wandinger, U., Bühl, J., & Engelmann, R. (2016). Relationship between temperature and apparent shape of pristine ice crystals derived from polarimetric cloud radar observations during the ACCEPT campaign. *Atmospheric Measurement Techniques*, *9*(8), 3739–3754. https://doi.org/10.5194/amt-9-3739-2016

Naso, A., Jucha, J., Lévêque, E., & Pumir, A. (2018). Collision rate of ice crystals with water droplets in turbulent flows. *Journal of Fluid Mechanics*, *845*, 615–641. https://doi.org/10.1017/jfm.2018.238

Nomokonova, T., Ebell, K., Löhnert, U., Maturilli, M., & Ritter, C. (2020). The influence of water vapor anomalies on clouds and their radiative effect at Ny-Å lesund. *Atmospheric Chemistry and Physics*, *20*(8), 5157–5173. https://doi.org/10.5194/acp-20-5157-2020

Ori, D., Schemann, V., Karrer, M., Dias Neto, J., von Terzi, L., Seifert, A., & Kneifel, S. (2020). Evaluation of ice particle growth in ICON using statistics of multi-frequency Doppler cloud radar observations. *Quarterly Journal of the Royal Meteorological Society*, *146*(733), 3830–3849. https://doi.org/10.1002/qj.3875

Pinsky, M. B., & Khain, A. P. (1998). Some effects of cloud turbulence on water–ice and ice–ice collisions. *Atmospheric Research*, *47*(48), 69–86. https://doi.org/10.1016/S0169-8095(98)00041-6

Prenni, A. J., Demott, P. J., Rogers, D. C., Kreidenweis, S. M., Mcfarquhar, G. M., Zhang, G., & Poellot, M. R. (2009). Ice nuclei characteristics from M-PACE and their relation to ice formation in clouds. *Tellus B: Chemical and Physical Meteorology*, *61*(2), 436–448. https://doi.org/10.1111/j.1600-0889.2009.00415.x

Pruppacher, H. R., & Klett, J. D. (2012). *Microphysics of clouds and precipitation: Reprinted 1980*. Springer. https://doi.org/10.1007/978-94-009-9905-3

Pumir, A., & Wilkinson, M. (2016). Collisional aggregation due to turbulence. *Annual Review of Condensed Matter Physics*, *7*(1), 141–170. https://doi.org/10.1146/annurev-conmatphys-031115-011538

Ramelli, F., Henneberger, J., David, R. O., Lauber, A., Pasquier, J. T., Wieder, J., et al. (2021). Influence of low-level blocking and turbulence on the microphysics of a mixed-phase cloud in an inner-Alpine valley. *Atmospheric Chemistry and Physics*, *21*(6), 5151–5172. https://doi.org/10.5194/acp-21-5151-2021

Rangno, A. L., & Hobbs, P. V. (2001). Ice particles in stratiform clouds in the Arctic and possible mechanisms for the production of high ice concentrations. *Journal of Geophysical Research*, *106*(D14), 15065–15075. https://doi.org/10.1029/2000JD900286

Rogers, R., & Tripp, B. (1964). Some radar measurements of turbulence in snow. *Journal of Applied Meteorology and Climatology*, *3*(5), 603–610. https://doi.org/10.1175/1520-0450(1964)003⟨0603:SRMOTI⟩2.0.CO;2

Saffman, P., & Turner, J. (1956). On the collision of drops in turbulent clouds. *Journal of Fluid Mechanics*, *1*(1), 16–30. https://doi.org/10.1017/S0022112056000020

Schrom, R. S., & Kumjian, M. R. (2016). Connecting microphysical processes in Colorado winter storms with vertical profiles of radar observations. *Journal of Applied Meteorology and Climatology*, *55*(8), 1771–1787. https://doi.org/10.1175/JAMC-D-15-0338.1

Schrom, R. S., Kumjian, M. R., & Lu, Y. (2015). Polarimetric radar signatures of dendritic growth zones within Colorado winter storms. *Journal of Applied Meteorology and Climatology*, *54*(12), 2365–2388. https://doi.org/10.1175/JAMC-D-15-0004.1

Schwarzenboeck, A., Shcherbakov, V., Lefevre, R., Gayet, J. F., Pointin, Y., & Duroure, C. (2009). Indications for stellar-crystal fragmentation in Arctic clouds. *Atmospheric Research*, *92*(2), 220–228. https://doi.org/10.1016/j.atmosres.2008.10.002

Seifert, A., Nuijens, L., & Stevens, B. (2010). Turbulence effects on warm-rain autoconversion in precipitating shallow convection. *Quarterly Journal of the Royal Meteorological Society*, *136*(652), 1753–1762. https://doi.org/10.1002/qj.684

Seifert, A., & Onishi, R. (2016). Turbulence effects on warm-rain formation in precipitating shallow convection revisited. *Atmospheric Chemistry and Physics*, *16*(18), 12127–12141. https://doi.org/10.5194/acp-16-12127-2016

Shaw, R. A. (2003). Particle-turbulence interactions in atmospheric clouds. *Annual Review of Fluid Mechanics*, *35*(1), 183–227. https://doi.org/10.1146/annurev.fluid.35.101101.161125

Shaw, R. A., Reade, W. C., Collins, L. R., & Verlinde, J. (1998). Preferential concentration of cloud droplets by turbulence: Effects on the early evolution of cumulus cloud droplet spectra. *Journal of the Atmospheric Sciences*, *55*(11), 1965–1976. https://doi.org/10.1175/1520-0469(1998)055⟨1965:PCOCDB⟩2.0.CO;2

Sheikh, M. Z., Gustavsson, K., Lévêque, E., Mehlig, B., Pumir, A., & Naso, A. (2022). Colliding ice crystals in turbulent clouds. *Journal of the Atmospheric Sciences*, *79*(9), 2205–2218. https://doi.org/10.1175/JAS-D-21-0305.1

Shupe, M. D., Kollias, P., Poellot, M., & Eloranta, E. (2008). On deriving vertical air motions from cloud radar Doppler spectra. *Journal of Atmospheric and Oceanic Technology*, *25*(4), 547–557. https://doi.org/10.1175/2007JTECHA1007.1

Shupe, M. D., Matrosov, S. Y., & Uttal, T. (2006). Arctic mixed-phase cloud properties derived from surface-based sensors at SHEBA. *Journal of the Atmospheric Sciences*, *63*(2), 697–711. https://doi.org/10.1175/JAS3659.1

Siebert, H., Lehmann, K., & Wendisch, M. (2006). Observations of small-scale turbulence and energy dissipation rates in the cloudy boundary layer. *Journal of the Atmospheric Sciences*, *63*(5), 1451–1466. https://doi.org/10.1175/JAS3687.1

Small, J. D., & Chuang, P. Y. (2008). New observations of precipitation initiation in warm cumulus clouds. *Journal of the Atmospheric Sciences*, *65*(9), 2972–2982. https://doi.org/10.1175/2008JAS2600.1

Squires, K. D., & Eaton, J. K. (1991). Preferential concentration of particles by turbulence. *Physics of Fluids A: Fluid Dynamics*, *3*(5), 1169–1178. https://doi.org/10.1063/1.858045

Takahashi, T. (2014). Influence of liquid water content and temperature on the form and growth of branched planar snow crystals in a cloud. *Journal of the Atmospheric Sciences*, *71*(11), 4127–4142. https://doi.org/10.1175/JAS-D-14-0043.1

19448007, 2024, 6, Downloaded from https://agupubs.onlinelibrary.wiley.com/doi/10.1029/2023GL106599 by Bibl. der Universitat zu Koln, Wiley Online Library on [12/11/2026]. See the Terms and Conditions (https://onlinelibrary.wiley.com/terms-and-conditions) on Wiley Online Library for rules of use; OA articles are governed by the applicable Creative Commons License

Tetoni, E., Ewald, F., Hagen, M., Köcher, G., Zinner, T., & Groß, S. (2022). Retrievals of ice microphysical properties using dual-wavelength polarimetric radar observations during stratiform precipitation events. *Atmospheric Measurement Techniques*, *15*(13), 3969–3999. https://doi.org/10.5194/amt-15-3969-2022

Trömel, S., Simmer, C., Blahak, U., Blanke, A., Doktorowski, S., Ewald, F., et al. (2021). Overview: Fusion of radar polarimetry and numerical atmospheric modelling towards an improved understanding of cloud and precipitation processes. *Atmospheric Chemistry and Physics*, *21*(23), 17291–17314. https://doi.org/10.5194/acp-21-17291-2021

Vaillancourt, P. A., & Yau, M. (2000). Review of particle-turbulence interactions and consequences for cloud physics. *Bulletin of the American Meteorological Society*, *81*(2), 285–298. https://doi.org/10.1175/1520-0477(2000)081⟨0285:ROPIAC⟩2.3.CO;2

Vogl, T., Maahn, M., Kneifel, S., Schimmel, W., Moisseev, D., & Kalesse-Los, H. (2022). Using artificial neural networks to predict riming from Doppler cloud radar observations. *Atmospheric Measurement Techniques*, *15*(2), 365–381. https://doi.org/10.5194/amt-15-365-2022

von Terzi, L., Dias Neto, J., Ori, D., Myagkov, A., & Kneifel, S. (2022). Ice microphysical processes in the dendritic growth layer: A statistical analysis combining multi-frequency and polarimetric Doppler cloud radar observations. *Atmospheric Chemistry and Physics*, *22*(17), 11795–11821. https://doi.org/10.5194/acp-22-11795-2022

Voßkuhle, M., Pumir, A., Lévêque, E., & Wilkinson, M. (2014). Prevalence of the sling effect for enhancing collision rates in turbulent suspensions. *Journal of Fluid Mechanics*, *749*, 841–852. https://doi.org/10.1017/jfm.2014.259

Wang, P. K., & Ji, W. (2000). Collision efficiencies of ice crystals at low–intermediate Reynolds numbers colliding with supercooled cloud droplets: A numerical study. *Journal of the Atmospheric Sciences*, *57*(8), 1001–1009. https://doi.org/10.1175/1520-0469(2000)057⟨1001:CEOICA⟩2.0.CO;2

Westbrook, C., Ball, R., Field, P., & Heymsfield, A. (2004). Theory of growth by differential sedimentation, with application to snowflake formation. *Physical Review E*, *70*(2), 021403. https://doi.org/10.1103/PhysRevE.70.021403

Zhao, C., & Garrett, T. (2008). Ground-based remote sensing of precipitation in the Arctic. *Journal of Geophysical Research: Atmospheres*, *113*(D14). https://doi.org/10.1029/2007JD009222

References From the Supporting Information

Brewster, K. A., & Zrnić, D. S. (1986). Comparison of eddy dissipation rates from spatial spectra of Doppler velocities and Doppler spectrum widths. *Journal of Atmospheric and Oceanic Technology*, *3*(3), 440–452. https://doi.org/10.1175/1520-0426(1986)003⟨0440:COEDRF⟩2.0.CO;2

Griesche, H. J., Seifert, P., Ansmann, A., Baars, H., Barrientos Velasco, C., Bühl, J., et al. (2020). Application of the shipborne remote sensing supersite OCEANET for profiling of Arctic aerosols and clouds during Polarstern cruise PS106. *Atmospheric Measurement Techniques*, *13*(10), 5335–5358. https://doi.org/10.5194/amt-13-5335-2020

Hildebrand, P. H., & Sekhon, R. (1974). Objective determination of the noise level in Doppler spectra. *Journal of Applied Meteorology and Climatology*, *13*(7), 808–811. https://doi.org/10.1175/1520-0450(1974)013⟨0808:ODOTNL⟩2.0.CO;2

Kiszler, T., Ebell, K., & Schemann, V. (2023). A performance baseline for the representation of clouds and humidity in cloud-resolving ICON-LEM simulations in the Arctic. *Journal of Advances in Modeling Earth Systems*, *15*(5), e2022MS003299. https://doi.org/10.1029/2022MS003299

Kollias, P., Albrecht, B., Lhermitte, R., & Savtchenko, A. (2001). Radar observations of updrafts, downdrafts, and turbulence in fair-weather cumuli. *Journal of the Atmospheric Sciences*, *58*(13), 1750–1766. https://doi.org/10.1175/1520-0469(2001)058⟨1750:ROOUDA⟩2.0.CO;2

O'Connor, E. J., Hogan, R. J., & Illingworth, A. J. (2005). Retrieving stratocumulus drizzle parameters using Doppler radar and lidar. *Journal of Applied Meteorology*, *44*(1), 14–27. https://doi.org/10.1175/JAM-2181.1

Pope, S. B. (2000). *Turbulent flows*. Cambridge University Press.

Schemann, V., & Ebell, K. (2020). Simulation of mixed-phase clouds with the ICON large-eddy model in the complex Arctic environment around Ny-Ålesund. *Atmospheric Chemistry and Physics*, *20*(1), 475–485. https://doi.org/10.5194/acp-20-475-2020

Shupe, M. D., Kollias, P., Persson, P. O. G., & McFarquhar, G. M. (2008). Vertical motions in Arctic mixed-phase stratiform clouds. *Journal of the Atmospheric Sciences*, *65*(4), 1304–1322. https://doi.org/10.1175/2007JAS2479.1

Zhu, Z., Kollias, P., & Yang, F. (2023). Particle inertia effects on radar Doppler spectra simulation. *Atmospheric Measurement Techniques*, *16*(15), 3727–3737. https://doi.org/10.5194/amt-16-3727-2023

19448007, 2024, 6, Downloaded from https://agupubs.onlinelibrary.wiley.com/doi/10.1029/2023GL106599 by Bibl. der Universitat zu Koln, Wiley Online Library on [12/11/2026]. See the Terms and Conditions (https://onlinelibrary.wiley.com/terms-and-conditions) on Wiley Online Library for rules of use; OA articles are governed by the applicable Creative Commons License